THE JOURNAL OF PHYSICAL CHEMISTRY Letters

Letter

pubs.acs.org/JPCL

Steric Effects of Solvent Molecules on S_N2 Substitution Dynamics

Xu Liu,[†] Jing Xie,[‡] Jiaxu Zhang,*[,†] Li Yang,*[,†] and William L. Hase[§]

[†]MIIT Key Laboratory of Critical Materials Technology for New Energy Conversion and Storage, School of Chemistry and Chemical Engineering, Harbin Institute of Technology, Harbin 150001, People's Republic of China

[‡]Department of Chemistry, University of Minnesota, Minneapolis, Minnesota 55455, United States

[§]Department of Chemistry and Biochemistry, Texas Tech University, Lubbock, Texas 79409, United States

ABSTRACT: Influences of solvent molecules on S_N2 reaction dynamics of microsolvated $F^-(H_2O)_n$ with CH_3I, for n = 0−3, are uncovered by direct chemical dynamics simulations. The direct substitution mechanism, which is important without microsolvation, is quenched dramatically upon increasing hydration. The water molecules tend to force reactive encounters to proceed through the prereaction collision complex leading to indirect reaction. In contrast to $F^-(H_2O)$, reaction with higher hydrated ions shows a strong propensity for ion desolvation in the entrance channel, diminishing steric hindrance for nucleophilic attack. Thus, nucleophilic substitution avoids the potential energy barrier with all of the solvent molecules intact and instead occurs through the less solvated barrier, which is energetically unexpected because the former barrier has a lower energy. The work presented here reveals a trade-off between reaction energetics and steric effects, with the latter found to be crucial in understanding how hydration influences microsolvated S_N2 dynamics.

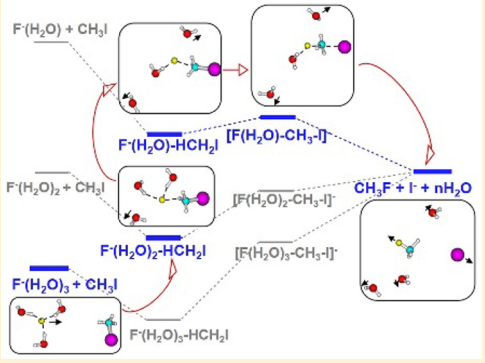

Bimolecular nucleophilic substitution (S_N2) reactions are of central importance in chemistry and biochemistry and continue to be the pivotal model systems in the field of chemical reaction kinetics and dynamics.[1,2] These reactions are widely used in preparative organic synthesis.[3] Low-energy negative-ion reactions, most likely nucleophilic substitution, are suggested to cause the large amount of DNA double strand breaks in the wake of ionizing particles.[4] Rather than identifying reaction products and measuring reaction rates, recent experimental and computational advances allow one to obtain insight into details of the underlying S_N2 dynamics.[2,5] Recently, the novel roundabout[6] and double inversion[7] mechanisms were discovered, which have attracted great current interest and enriched modern understanding of the S_N2 reaction mechanism.

There have been extensive studies of gas-phase $X^- + CH_3Y$ reactions,[8−10] in particular, the nonstatistical and nontraditional dynamics found for the S_N2 pathway.[7,11] However, the dynamics in the liquid phase is more complex and much different,[12,13] where nonequilibrium solvation effects may be of great significance.[14,15] As a bridge between the gas phase and solution, microsolvation has received particular attention, which offers a bottom-up approach to investigate details of interactions between the S_N2 reactants and solvent.[12,16−18] In general, solvation stabilizes the reactants more than it does the transition state (TS) located at the central barrier.[18,19] This stabilization therefore leads to an increased barrier height that hinders reaction. As a result, rate constants are often observed to decrease substantially with increasing solvation.[12,20,21] The effect of solvation is usually considered to be governed by thermodynamics. In contrast, little is known about the dynamical and steric effects caused by the individual solvent molecules. Lately, molecular beam, ion-imaging experiments for $OH^-(H_2O)_n + CH_3I$ reactions with n = 0−2 have shown that the stepwise hydration of OH^- alters the reaction dynamics and kinetics quite remarkably from those for the corresponding bare ion.[22] Furthermore, the results suggest that the steric characteristics are at least as relevant as energetics in understanding the influence of solvent molecules in such microsolvated reactions. Chemical dynamics simulations provided an atomistic interpretation of these experiments and probed the role of the H_2O molecule.[23]

The influence of microsolvation on chemical reactivity is often based on stationary points on the reaction's potential energy surface (PES). This usually provides limited insight into the underlying dynamics because atomistic details of the reaction mechanisms may deviate substantially from those predicted by stationary points and the intrinsic reaction coordinate (IRC),[24] which are only uncovered by chemical dynamics simulations.[11] Trajectory calculations for $F^-(H_2O)_{0,1} + CH_3I$ reactions[25−27] have successfully reproduced the experimental findings[26,28] and revealed that the S_N2 reaction occurs by overcoming the potential energy barrier on the PES's IRC (see Figure 1). However, in the current study, we find that the higher hydrated reactions do not follow their IRC profiles, which have TSs with all of the water molecules interacting with the reactive system. Instead, the reactions tend to dehydrate, crossing a S_N2 TS with less solvation. This is very interesting

Received: March 8, 2017
Accepted: April 10, 2017
Published: April 10, 2017

DOI: 10.1021/acs.jpclett.7b00577
J. Phys. Chem. Lett. 2017, 8, 1885−1892

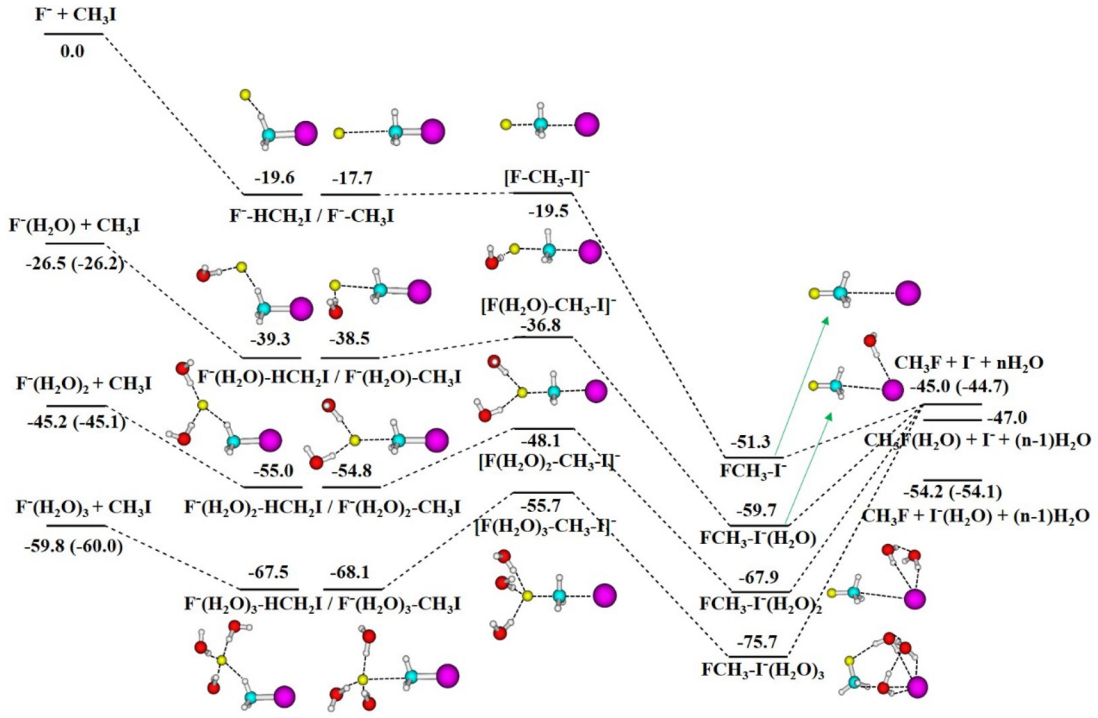

Figure 1. Schematic energy profiles and stationary points for the $F^-(H_2O)_{n=0-3}$ + CH_3I reactions at the B3LYP/ECP/d level of theory. The energies in kcal/mol are relative to isolated molecules and ions and include the zero-point energy (ZPE). Experimental data in parentheses are from refs 36−38. The results for n = 0 and 1 were presented previously.[27,31] B3LYP single-point energy for the MP2 optimized structure is given for the nonhydrated $[F{-}CH_3{-}I]^-$ TS and $F^-{-}CH_3I$ complex, which failed to be located with DFT theory due to the rather flat prereaction region of the PES.[31]

because this pathway has a higher barrier than the one with all of the H_2O molecules intact. To understand how this occurs, in the following, we explore reaction mechanisms for the $F^-(H_2O)_n$ + CH_3I (n = 0−3) prototypical S_N2 reactions. Atomistic dynamics is compared for an increasing degree of hydration and found to signify a trade-off between steric effects and reaction energetics for the influence of solvation on the chemical reaction. The present work sheds light on how solute−solvent interactions affect the underlying reaction dynamics at a deeper atomic level, which remains largely unclear.

Chemical dynamics simulations require an accurate PES, which governs the motion of the atoms for the chemical reaction. PES profiles for the $F^-(H_2O)_n$ + CH_3I S_N2 reactions, with n up to 3 at the B3LYP/ECP/d level of theory,[29] are characterized in Figure 1. The ECP/d[30] basis set has been defined in previous work[23,31,32] and proven to be successful in dealing with the S_N2 reactions involving iodine.[23,25−27,31−34] Different electronic structure theories and basis sets have been employed to probe the stationary point properties of the monosolvated $F^-(H_2O)$ reaction, and the B3LYP/ECP/d results were found to give the best agreement with available experimental and benchmark CCSD(T) data.[35] For the current higher-order hydrated systems, the B3LYP/ECP/d method also performs well when compared with experimental reaction energies and solvation energies[36−38] (Figure 1) and is chosen for the direct dynamics simulations reported here.

The initial association of $F^-(H_2O)_n$ and CH_3I may form either a hydrogen-bonded $F^-(H_2O)_n{-}HCH_2I$ (im1) or an ion−dipole $F^-(H_2O)_n{-}CH_3I$ (im2) prereaction complex without an activation barrier. Afterward, the complex overcomes the corresponding S_N2 TS $[F(H_2O)_n{-}CH_3{-}I]^-$ (TS1) and undergoes the substitution reaction with Walden inversion to the postreaction complex $FCH_3{-}I^-(H_2O)_n$ (im3). The dissociation of the complex (im3) leads to either bare I^- and CH_3F products or hydrated ones. This profile is in line with the qualitative potential model of microsolvated S_N2 reactions proposed by Brauman et al.[39] As the nucleophile is hydrated more, the prereaction complex becomes less stable and the overall barrier higher. More detailed electronic structure theory calculations for the $F^-(H_2O)_n$ + CH_3I PES profiles and the stationary point properties will be given in a forthcoming publication.

With chemical dynamics simulations, which give atomistic motions for the chemical reaction, one can go much further than predicting reaction mechanisms based on stationary points. In the current study, simulations for the reactions $F^-(H_2O)_n$ + CH_3I were performed for the di- and trihydrates (n = 2, 3) employing a direct dynamics method[31] at the B3LYP/ECP/d level of theory. The $F^-(H_2O)_2$ results are reported for a 0.32 eV collision energy (E_{coll}) and vibrational and rotational temperatures (T_v/T_r) of 360/75 K for CH_3I and 100/100 K for $F^-(H_2O)_2$ to compare with the previous $F^-(H_2O)_{0,1}$ reaction dynamics.[26,27] The S_N2 product channels, for the more hydrated $F^-(H_2O)_3$ reaction, open at higher collision energies (Figure 1). Thus, the $F^-(H_2O)_3$ dynamics calculations were carried out with the same T_v/T_r for the reactants as that for the two-water system but for a greater E_{coll} of 1.53 eV. This E_{coll} was also considered for the water-free studies.[26] Trajectories were propagated with the VENUS chemical dynamics computer program[40,41] interfaced to the NWChem electronic structure computer program.[42]

At a low collision energy of 0.32 eV, the solvent-free F^- + CH_3I reaction (R0) gives the unique products CH_3F + I^-.

DOI: 10.1021/acs.jpclett.7b00577
J. Phys. Chem. Lett. 2017, 8, 1885−1892

Solvating the reactant species opens up new S_N2 pathways leading to solvated products. For the $F^-(H_2O)_{n=1,2}$ + CH_3I reactions (R1 and R2), three major product channels P1−P3 are observed, which amount to more than 90% of the substitution events. The zero-point energy (ZPE) corrected reaction energies (ΔE in kcal/mol) of the different channels are as follows on the B3LYP/ECP/d PES

$$F^- + CH_3I \rightarrow CH_3F + I^- \quad -45.0\ (R0)$$

$$F^-(H_2O)_n + CH_3I \rightarrow CH_3F + I^- + nH_2O \quad P1 \quad -18.5\ (n = 1, R1)$$

$$0.2\ (n = 2, R2)$$

$$\rightarrow CH_3F + I^-(H_2O) + (n-1)H_2O \quad P2 \quad -27.7\ (n = 1, R1)$$

$$-9.0\ (n = 2, R2)$$

$$\rightarrow CH_3F(H_2O) + I^- + (n-1)H_2O \quad P3 \quad -20.5\ (n = 1, R1)$$

$$-1.8\ (n = 2, R2)$$

Although P2 and P3 for solvated $I^-(H_2O)$ and $CH_3F(H_2O)$ are more favored in energy than P1, the former two products are strongly suppressed in reactions R1 and R2, as observed for almost all microsolvated $X^-(H_2O)_n$ + CH_3Y reactions.[16,17,21,22,28] Trajectory calculations indicate that the water molecule shows a propensity for departure from the reactive system as a result of efficient intramolecular vibrational energy redistribution (IVR), which is important for understanding the dynamics.[27] The branching ratio of P1/P2/P3 is determined to be 0.86:0.08:0.06 and 0.73:0.13:0.14 for n = 1[27] and 2, respectively, at E_{coll} = 0.32 eV. As discussed in more detail below, the corresponding ratio for n = 3 is 0.80:0.07:0.13 at a larger E_{coll} of 1.53 eV. For reactions with n = 1 and 2 studied at the same 0.32 eV collision energy, the fractions of the solvated products P2 and P3 increase with the stepwise hydration because the departing water molecule carries part of the available energy, and thus, fewer $I^-(H_2O)$ and $CH_3F(H_2O)$ products have an internal energy larger than the threshold energy for losing H_2O. This dependence of the P1/P2/P3 branching on n is in line with previous experiments for $X^-(H_2O)_n$ + CH_3Br (X = OH and F).[43,44]

Bierbaum et al. estimated the product anion ratio of I^-/$I^-(H_2O)$ for reaction R1 using the FA-SIFT technique, and the resulting value is 0.9/0.1 for reactants at a 300 K thermal energy (~0.04 eV).[28] The monohydrated $F^-(H_2O)$ + CH_3I dynamics has been investigated with trajectory simulations, which agrees well with experiment, giving an $I^-/I^-(H_2O)$ ratio of 0.92/0.08 at both 300 K and 0.32 eV, independent of E_{coll}.[27,33] The simulations indicate that the I^- ion is formed via channel P1 with minor contributions from channel P3. It is of interest that the relative I^- and $I^-(H_2O)$ fraction of 0.87:0.13 at 0.32 eV for reaction R2, obtained from our calculations, is consistent with the experiments and simulations for the isoelectronic $OH^-(H_2O)_2$ + CH_3I reaction giving 0.90:0.10 at ~300 K.[32]

The opacity functions, that is, the total reaction probability $P_r(b)$ as a function of the impact parameter b for reactions R0,[26] R1,[27] and R2, are compared in Figure 2. $P_r(b)$ extends to similarly large maximum impact parameters (b_{max}) of around 8−9 Å for n values of 0−2. Nonetheless, it decreases essentially with stepwise addition of a water molecule. Accordingly, the reaction cross section σ_r, obtained by integrating $P_r(b)$ over the impact parameter ($\int P_r(b) 2\pi b\, db$), diminishes appreciably and is 108.7 ± 9.7,[26] 25.1 ± 3.9,[27] and 6.3 ± 1.3 Å^2 for R0, R1, and R2, respectively. At E_{coll} of 0.32 eV studied here, the calculated cross sections give respective rate constants of $k(E_{coll}, T_v, T_r)$ =

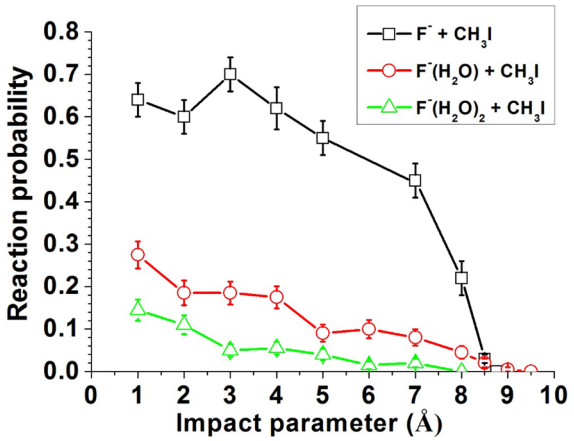

Figure 2. Reaction probabilities $P_r(b)$ for the $F^-(H_2O)_n$ + CH_3I (n = 0−2) reactions as a function of impact parameter b at a 0.32 eV collision energy. The $P_r(b)$ values of n = 0 and 1 are from refs 26 and 27, respectively. A total of 1250, 2200, and 1600 trajectories were calculated for n = 0−2, respectively, and the vertical error bars represent the statistical uncertainty in the reaction probability at each b, computed from the square root of the number of reactive events.

$v(E_{coll})\sigma(E_{coll}, T_v, T_r)$ = (2.0 ± 0.2) × 10^{-9}, (3.6 ± 0.6) × 10^{-10}, and (0.79 ± 0.17) × 10^{-10} cm^3 mol^{-1} s^{-1}. The unsolvated rate agrees very favorably with the experimental value at this energy of 1.7 × 10^{-9} cm^3 mol^{-1} s^{-1}.[45] For the monohydrated case, the trajectories at 300 K (~0.04 eV) are about twice as reactive as those at 0.32 eV.[27,33] The 300 K trajectory rate constant[33] of (7.4 ± 0.9) × 10^{-10} cm^3 mol^{-1} s^{-1} is in quite good agreement with the measured 300 K value[28] of (8.6 ± 0.1) × 10^{-10} cm^3 mol^{-1} s^{-1}.

The decrease in the 0.32 eV reactivity, with hydration of F^- with one water, is an approximate factor of 5. Adding a second water reduces the reactivity by another factor of 5. The experimental rate constants for isoelectronic $OH^-(H_2O)_n$ + CH_3I have been recently reported at 398 K (~0.05 eV), and the values are 1.9 × 10^{-9}, (9.1 ± 1.7) × 10^{-10}, and (0.84 ± 0.22) × 10^{-10} cm^3 mol^{-1} s^{-1} for n = 0−2.[32] The measured rate drops by a factor of 2 in going from n = 0 to 1 compared to a decrease of a factor of 10 in going from n = 1 to 2, a trend resembling that found here for the $F^-(H_2O)_n$ + CH_3I reactions at 0.32 eV. Variation of the collision energy affects the reactivity for these hydrated systems, while their reactivity is only weakly dependent on the vibrational and rotational temperatures T_{vr}.[32,34,45]

The suppression of reactivity with the addition of waters observed here for the $F^-(H_2O)_n$ + CH_3I reactions may well be correlated with the less submerged S_N2 barrier upon progressive hydration.[12] However, the atomistic dynamics for the more solvated systems, as discussed in detail below, involves desolvation. Instead of following the IRC with full solvation in the saddle point region, the displacement reaction may proceed through the less hydrated reaction path. Thus, the S_N2 barrier height ascribed to a TS with full hydration is likely not the only factor of importance in the reaction rate determination, when more solvent molecules are involved and desolvation becomes energetically accessible.

The simulations reveal three types of mechanisms for S_N2 reactions of CH_3I with the $F^-(H_2O)_{n=0-2}$ clusters, that is, direct rebound, direct stripping, and indirect mechanisms. Direct mechanisms do not follow the IRC reaction path, with the system trapped in either pre- or postreaction complex. The

DOI: 10.1021/acs.jpclett.7b00577
J. Phys. Chem. Lett. 2017, 8, 1885−1892

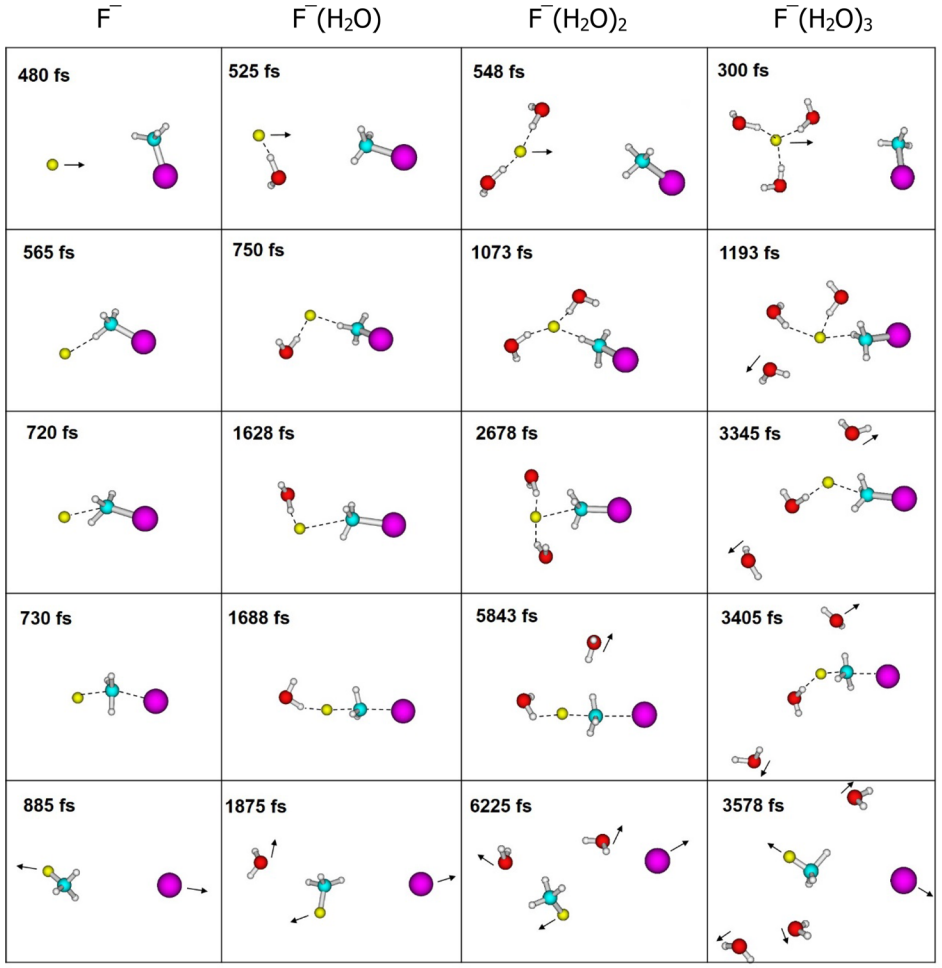

Figure 3. Atomistic dynamics of typical trajectories illustrating the dominant indirect mechanism for the $F^-(H_2O)_n + CH_3I \rightarrow CH_3F + I^- + nH_2O$ (n = 0−3) S_N2 reactions that forms an intermediate in the $F^-(H_2O)_n$–HCH_2I and $F^-(H_2O)_n$–CH_3I prereactive potential energy well. Results of n = 0−2 are for a collision energy of 0.32 eV, with that of n = 3 at a higher 1.53 eV. Snapshots of the F^- and $F^-(H_2O)$ trajectories are adapted from refs 25 and 27, respectively.

longest period of time of direct trajectories is around 2.3 ps, attributed to a relatively lower 0.32 eV collision energy. Rebound occurs at small impact parameters, for which $F^-(H_2O)_n$ strikes the backside of CH_3I and directly displaces I^-, resulting in backward scattering. Stripping becomes important for large impact parameters, where $F^-(H_2O)_n$ approaches CH_3I from the side and directly strips away the CH_3 group, giving forward scattering. The indirect mechanism is complex-mediated and covers a broad impact parameter range up to b_{max}, in which the reactants are usually trapped in the entrance channel, forming hydrogen-bonded and ion−dipole prereaction complexes, which comprise approximately 80−90% of the n = 0−2 indirect reactive trajectories. These two complexes frequently transform between each other, as expected given the small barrier between them.[27,31] Long-time retention in this complex region allows extensive overall rotation of the system, randomizing the scattering distributions. Complex formation in the product exit channel is less important with respect to that in the entrance channel and contributes mostly for n = 2, ∼15% of the indirect reaction. The very interesting roundabout mechanism[6] and frontside $F^-(H_2O)_n$–ICH_3 halogen-bonded complex are observed as well but found to play an insignificant role in the dynamics, which account for not more than 3% of the reactive events. This dominance of indirect dynamics proceeding through the prereaction complexes was also found for the isoelectronic $OH^-(H_2O)_{n=0-2}$ + CH_3I reactions.[23,32] Detailed dynamics of the water molecules for different atomistic mechanisms are discussed below.

For reactions R0,[26] R1,[27] and R2, the respective fractions of the direct rebound, direct stripping, and indirect mechanisms are 0.18:0.23:0.59, 0.14:0.15:0.71, and 0.02:0:0.98 at E_{coll} = 0.32 eV. This clearly shows indirect is the principle mechanism for each level of the n = 0−2 hydration, with the addition of each H_2O leading to a greater indirect fraction. The fractions of different mechanisms show a substantial change between n = 1 and 2 compared to that between n = 0 and 1. A detailed discussion given below suggests that in the reactive collisions of CH_3I with $F^-(H_2O)_2$ clusters, the steric hindrance prevails over energetics and becomes more pronounced than that in the $F^-(H_2O)$ case. The water molecules have to be pushed aside before the F^- can attack the substrate or the reaction has to proceed via a long-lived collision complex where the water molecules are shifted around or sheared off before substitution. As a result, the direct nucleophilic displacement mechanisms are strongly suppressed with two waters bound to the reactant ion. As illustrated below, the corresponding fraction for n = 3 is 0:0:1 at a larger collision energy of 1.53 eV. These systematic

DOI: 10.1021/acs.jpclett.7b00577
J. Phys. Chem. Lett. 2017, 8, 1885−1892

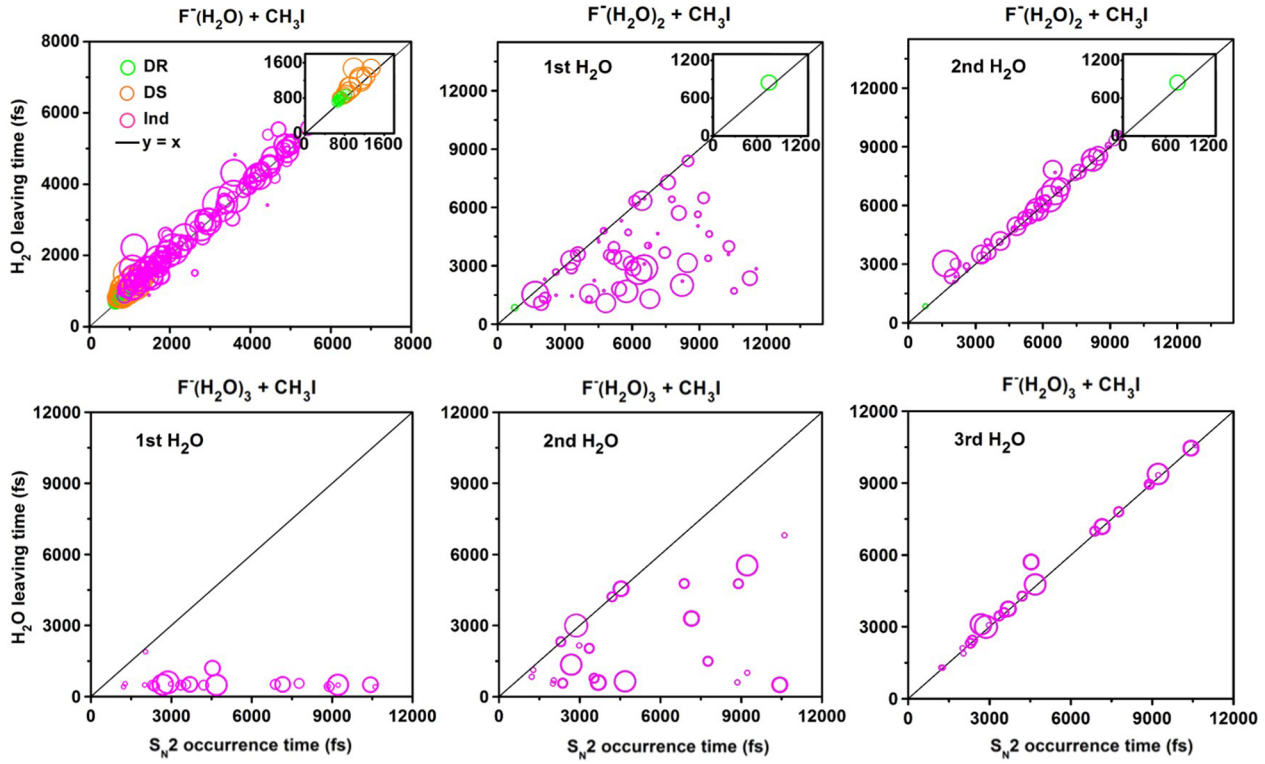

Figure 4. Scatter plot of the H_2O leaving time versus S_N2 occurrence time for the $F^-(H_2O)_n + CH_3I \rightarrow CH_3F + I^- + nH_2O$ S_N2 reactions, with n = 1−3. The H_2O leaving time is determined when the increasing HOH···X (X = F or I) distance between the departing H_2O and the reactive system reaches ∼2.2 Å, and the S_N2 occurrence time is recorded once the reactive system crosses the S_N2 barrier (see the text for details). Data of n = 1 and 2 at a 0.32 eV collision energy are depicted in the top row, and those for n = 3 at 1.53 eV are given in the bottom row. The results are shown for individual reaction mechanisms: DR, direct rebound; DS, direct stripping; Ind, indirect. For clarity, the information on DR and DS is also presented in the inset. Results for $F^-(H_2O) + CH_3I$ were presented in ref 33.

trends predict that for the higher hydrates solvation quenches direct events and indirect trajectories govern the displacement dynamics, as seen in molecular beam ion-imaging experiments for the isoelectronic $OH^-(H_2O)_{n=0-2}$ reactions.[22] Atomistic snapshots illustrating the indirect mechanism, with entrance channel complex formation that dominates the $F^-(H_2O)_n + CH_3I$ reactions, are depicted in Figure 3.

The time that H_2O leaves (i.e., dissociates from) the reactive system is an important component of the solvating water dynamics. This information is illustrated in Figure 4 for the primary product channel P1 of the S_N2 reactions R1 and R2, where the time that H_2O leaves is given as a scatter plot versus the time that the S_N2 reaction occurs. For the current $F^-(H_2O)_n + CH_3I$ reactions, the water molecule is attached to the reactive system via a HOH···X (X = F or I) hydrogen bond (see Figure 1), and the time that it leaves the system is determined when the increasing HOH···X distance between departing H_2O and the reactive system reaches ∼2.2 Å, the upper bound for a typical hydrogen bond length.[46] The time that the S_N2 reaction occurs is recorded once the reactive system crosses the potential energy barrier for F^- displacement of I^- and the S_N2 product CH_3F is formed. For monohydrated R1, ∼70% of the reaction is indirect. For the combined direct and indirect events, ∼90% occur with H_2O leaving as the S_N2 reaction occurs; that is, H_2O departure is simultaneous with CH_3F formation. H_2O does not depart before the S_N2 TS is reached and, thus, H_2O solvates the TS but not the I^- product. The influence of the water molecule on substitution dynamics given below shows that the monohydrated $F^-(H_2O) + CH_3I$ reaction occurs through the S_N2 barrier with one water attached. Once crossing the barrier and upon the formation of the C−F bond, the hydrogen bonding between H_2O and F (HOH···F) becomes weak and the energy released to the H···F stretch mode tends to break the hydrogen bonding, leading to water detachment.

The dynamics are much different for R2, where 98% of the reaction is indirect. For direct reaction, the loss of both H_2O molecules and the occurrence of the S_N2 reaction are simultaneous. For the indirect events, prereaction complex formation dominates, and the simulations reveal that for the majority of the trajectories (i.e., more than 80%) one H_2O leaves before the S_N2 reaction occurs, whereas the second one interacts with the reactive system for a longer period of time up to the occurrence of the S_N2 reaction or after the reaction occurs. For the remaining indirect trajectories, the departure of both H_2O molecules is nearly simultaneous with the S_N2 displacement. Thus, for the doubly hydrated $F^-(H_2O)_2 + CH_3I$ system, there is a strong propensity for one H_2O to leave the reactive system before the S_N2 reaction occurs, which probably has multiple origins. As described below, an important water molecule stereochemical factor may be partly responsible for the observed H_2O dynamics.

The simulations shed light on steric effects besides energetics in understanding the influence of solvent molecules on the substitution dynamics. With one water bound to the fluoride ion, direct propagation of the nucleophile to the TS is hindered, with direct substitution less probable than that for the unsolvated case. As discussed above for reaction R1, indirect events increase with formation of the microsolvated $F^-(H_2O)$−HCH_2I/$F^-(H_2O)$−CH_3I prereaction complex and dominate

DOI: 10.1021/acs.jpclett.7b00577
J. Phys. Chem. Lett. 2017, 8, 1885−1892

the reaction. With ZPE included, from Figure 1, it is seen that the energy of this solvated prereaction complex is approximately 39 kcal/mol lower than that of the unsolvated H_2O + F^- + CH_3I reactants. The microsolvation energy of this complex, that is, the energy difference between the n = 1 solvated and unsolvated F^-−HCH_2I/F^-−CH_3I complex, is ∼20 kcal/mol and less than the 26.5 kcal/mol microsolvation energy of F^-. The total energy available in the simulation of the n = 1 prereaction complex is the collision energy E_{coll}, the potential energy release in its formation and the small thermal energy of reactants, whose combined value is around 22.0 kcal/mol at E_{coll} of 0.32 eV, slightly greater than the complex's ∼20 kcal/mol microsolvation energy. This suggests that desolvation of the $F^-(H_2O)$−HCH_2I/$F^-(H_2O)$−CH_3I complex is energetically available. However, instead of losing H_2O, the vast majority of the trajectories that proceed through this complex pass over the n = 1 saddle point and form the CH_3F + I^- + H_2O products. This is in accord with the 17.3 kcal/mol higher unsolvated versus solvated energy barrier. Also, the above water dynamics for the indirect $F^-(H_2O)$ + CH_3I trajectories shows that H_2O remains attached to F^- until the S_N2 reaction occurs and then dissociates. These results indicate that the involvement of only one water is not enough to frustrate the nucleophilic reaction with F^- solvated. Energetics play an important part in the monosolvated dynamics.

Adding a second water molecule to the reactant ion introduces more steric crowding, and 98% of the R2 reaction proceeds via an indirect mechanism dominated by prereaction complex formation, from which the water molecules need to be pushed aside before F^- can attack the substrate. The energy of the two-water prereaction complex relative to the energy of $2H_2O$ + F^- + CH_3I is −55.0 kcal/mol, yielding an energy of microsolvation for n = 2 of ∼36 kcal/mol. The energy of desolvation for the n = 2 complex going to the n = 1 complex is 16.0 kcal/mol, larger than the energy barrier of 6.9 kcal/mol from the n = 2 complex to the saddle point. At E_{coll} of 0.32 eV studied here, the energy available for the n = 2 complex is ∼19.0 kcal/mol, and its desolvation to the n = 1 complex with consequential displacement via the n = 1 saddle point is energetically accessible.

Most n = 2 reactive trajectories (87%) enter the potential well for the prereaction complex and then show a clear preference for the above desolvation pathway for the CH_3F + I^- + $2H_2O$ reaction products. The water dynamics for $F^-(H_2O)_2$ + CH_3I reveals that one H_2O tends to break away from the reactive system at an early stage of the trajectory, but the other departs as the substitution reaction occurs. This is a quite interesting result, considering that the displacement through the two-water solvated TS is energetically more favored by 11.3 kcal/mol.

The relative ratio of the trajectories that follow the two pathways, that is, n = 2 complex → n = 1 complex → n = 1 TS and n = 2 complex → n = 2 TS, as found from simulations, is 0.71:0.16, illustrating that steric effects of the water molecules prevail over energetics in the $F^-(H_2O)_2$ + CH_3I system, and the dehydration pathway with one less solvent molecule to block the nucleophile is favored for the S_N2 channel. For a small fraction of the trajectories (11%), the reactant collision leads to separation of one H_2O from $F^-(H_2O)_2$. The reactive system enters the prereaction potential well of the one-water complex and then escapes through the one-water saddle point to the product asymptote. This tends to be a high collision energy event and is also observed for the $OH^-(H_2O)$ + CH_3I reaction.[23] This indirect reaction is similar to the $X^-(H_2O)_n$ + CH_3Y → $X^-(H_2O)_{n-1}(CH_3Y)$ + H_2O ligand switching mechanism proposed by Viggiano and co-workers upon ion solvation with 1−3 water molecules.[47]

Considering Figure 1, we see that hydration progressively enhances the S_N2 barrier and the reaction energies. The prominent product channel P1 of solvent-free species already becomes slightly endothermic for n = 2. For the higher hydrates ($n \geq 3$), the reaction becomes more endothermic and higher collision energies are required for the S_N2 reaction to occur with desolvation of the product ion. Both desolvation of the prereaction complex and ligand switching pathways followed by substitution via the less solvated S_N2 TS are open. These are expected to be the dominant mechanisms upon increasing hydration.

To confirm these assumptions, the $F^-(H_2O)_3$ + CH_3I dynamics was probed for a higher E_{coll} of 1.53 eV, the same energy used for unsolvated experiments and simulations.[26] In accordance with the lower hydrates, a complete desolvation pathway leading to the high-energy P1 CH_3F + I^- + $3H_2O$ (ΔE = 14.8 kcal/mol) governs the $F^-(H_2O)_3$ reaction, comprising ∼80% of the substitution dynamics, whereas the solvated products P2 CH_3F + $I^-(H_2O)$ + $2H_2O$ (ΔE = 5.6 kcal/mol) and P3 $CH_3F(H_2O)$ + I^- + $2H_2O$ (ΔE = 12.8 kcal/mol) play a minor role with respective contributions of 7 and 13%. As expected, "blocking" by the water molecules greatly enhances indirect reaction for $F^-(H_2O)_3$ and direct events are negligible. Interestingly, almost all of the $F^-(H_2O)_3$ trajectories do not follow the three-water IRC reaction path model shown in Figure 1. Instead, ligand switching occurs in the early stage of the reaction, that is, high-energy collisions between the two reactants result in one or two H_2O molecules dissociating from $F^-(H_2O)_3$. Of these trajectories, ∼22% enter the $F^-(H_2O)$−HCH_2I/$F^-(H_2O)$−CH_3I prereaction potential energy well, forming a reaction intermediate, and subsequently escape through the $[F(H_2O)$−CH_3−$I]^-$ TS, with one water attached, followed by direct fragmentation to the CH_3F + I^- + $3H_2O$ products.

The remaining 78% of $F^-(H_2O)_3$ trajectories become temporarily trapped in the two-water $F^-(H_2O)_2$−HCH_2I/$F^-(H_2O)_2$−CH_3I potential energy well after the reactants' initial collision, for which two reaction pathways are identified. For one, the trajectories follow the IRC of the $F^-(H_2O)_2$ reaction up to the two-water $[F(H_2O)_2$−CH_3−$I]^-$ TS but then move off of the IRC after passing the TS and form the desolvated products instead of going into the deep FCH_3−$I^-(H_2O)_2$ potential energy minimum. Only 20% of the trajectories, forming the two-water prereaction complex, are of this type. In contrast, all of the remaining trajectories prefer the second pathway with one water further detached. The system then enters the $F^-(H_2O)$−HCH_2I/$F^-(H_2O)$−CH_3I potential well and undergoes the S_N2 reaction after bypassing the one-water TS, as depicted in the right-most panels of Figure 3. In this way, the steric hindrance by the water molecule is diminished, thereby favoring the F^- nucleophilic attack, even though the pathway of n = 2 complex → n = 1 complex → n = 1 TS is not preferred in energetics compared to that following n = 2 complex → n = 2 TS (see Figure 1). This dynamics parallels the above $F^-(H_2O)_2$ dynamics, which pick the high-energy pathway of prereaction complex dehydration. Notably, the less solvated S_N2 reaction pathways are energetically not accessible for the $F^-(H_2O)_3$ + CH_3I at a lower E_{coll} = 0.32 eV. Even though the $I^-(H_2O)$ solvated product channel through

DOI: 10.1021/acs.jpclett.7b00577
J. Phys. Chem. Lett. 2017, 8, 1885−1892

the S_N2 barrier with full solvation opens, a preliminary calculation showed that none of the propagated trajectories form the $I^-(H_2O)$ reaction product, suggesting that it might be sterically hindered and therefore suppressed.

The propensity for less hydrated pathways is seen in the water dynamics diagram in Figure 4 (lower panels). The first water molecule leaves F^- early, arising from collision-induced desolvation, followed quickly by dissociation of a second H_2O molecule to some extent. As shown in the middle lower panel of Figure 4, for the remaining $F^-(H_2O)_2$ ions, most of the second water molecules desolvate as $F^-(H_2O)_2$ and CH_3I interact in the entrance channel, with a minor fraction staying attached to F^- and then being sheared off upon formation of the C−F bond. The third H_2O keeps interacting with the reactive system for longer times, with its departure approximately simultaneous with the displacement reaction. Overall, the trajectories reveal that the $F^-(H_2O)_3$ dynamics shows a strong propensity of desolvation before the reactive system reaches the reaction's dynamical bottleneck, which essentially reduces the steric crowding and thereby facilitates the attack of F^- at CH_3I.

The direct dynamics simulation reported here provides important fundamental information concerning atomic-level S_N2 dynamics under microsolvation. Overall, the prereaction complexes are found to play a decisive role in the $F^-(H_2O)_{n=0-3}$ + CH_3I dynamics. However, the large energy release in the exit channel contributes to rapid separation of the product species without significant postcollision interaction, which is supported by the experimental observation that the energetically favored solvated product is strongly suppressed with respect to the bare one.[16,21,22,28]

Quite interestingly, for reactive $F^-(H_2O)_2$ trajectories, there is preferential one H_2O loss and desolvation of the complex in the entrance channel. Then, the reactive system passes over the potential energy barrier with only one H_2O attached, which is higher in energy than the barrier with solvation by both H_2O molecules. This suggests that steric characteristics may have fundamental influences on the reaction dynamics in the presence of two waters. The substitution reaction for the more sterically "crowded" $F^-(H_2O)_3$ requires higher energies, where the reactants' collision induces desolvation with the majority of the trajectories transiently trapped in the $F^-(H_2O)_2$−HCH_2I/$F^-(H_2O)_2$−CH_3I prereaction potential well. Then, atomistic motions of these trajectories show similar behavior as that for the $F^-(H_2O)_2$ reaction, which tends to eject one water molecule and then follow the $F^-(H_2O)$ S_N2 pathway.

It is reasonable to assume that upon further solvation of the ionic reactant, steric hindrance by the water molecules will force all reactive encounters to proceed through an indirect mechanism involving prereaction complex formation, which will become a critical factor affecting the solvated S_N2 dynamics. A general component for larger hydrated clusters is expected to feature dynamics in which solvating waters are ejected, even though these pathways require energy. In this way, the solvation shell of the nucleophile is partially stripped away, thereby efficiently facilitating the succeeding S_N2 displacement. Further work is being carried out, over a wide range of collision energies, on more highly hydrated reactions as well as on effects of different solvent molecules. The present findings enrich our understanding of the nucleophilic substitution dynamics under microsolvation and may pave the way for exploration of complex solvent effects on chemical reactions proceeding in solution.

AUTHOR INFORMATION

Corresponding Authors

*E-mail: zhjx@hit.edu.cn (J.Z.).
*E-mail: yangli2014@hit.edu.cn (L.Y.).

ORCID

Li Yang: 0000-0002-0143-3524
William L. Hase: 0000-0002-0560-5100

Notes

The authors declare no competing financial interest.

ACKNOWLEDGMENTS

This work is supported by the National Natural Science Foundation of China (Nos. 21573052, 21403047, 51536002) and the Fundamental Research Funds for the Central Universities, China (AUGA5710012114, 5710012014). The research of W.L.H. reported here is based upon work supported by the Robert A. Welch Foundation under Grant No. D-0005. Support is also provided by the High Performance Computing Center (HPCC) at Texas Tech University, under the direction of Philip W. Smith.

REFERENCES

(1) Chabinyc, M. L.; Craig, S. L.; Regan, C. K.; Brauman, J. I. Gas-Phase Ionic Reactions: Dynamics and Mechanism of Nucleophilic Displacements. *Science* **1998**, *279*, 1882−1886.
(2) Xie, J.; Hase, W. L. Rethinking the S_N2 Reaction. *Science* **2016**, *352*, 32−33.
(3) Merceron-Saffon, N.; Baceiredo, A.; Gornitzka, H.; Bertrand, G. Synthesis of Carbenes Through Substitution Reactions at a Carbene Center. *Science* **2003**, *301*, 1223−1225.
(4) Boudaiffa, B.; Cloutier, P.; Hunting, D.; Huels, M. A.; Sanche, L. Resonant Formation of DNA Strand Breaks by Low-Energy (3 to 20 eV) Electrons. *Science* **2000**, *287*, 1658−1660.
(5) Stei, M.; Carrascosa, E.; Kainz, M. A.; Kelkar, A. H.; Meyer, J.; Szabó, I.; Czakó, G.; Wester, R. Influence of the Leaving Group on the Dynamics of a Gas-Phase S_N2 Reaction. *Nat. Chem.* **2016**, *8*, 151−156.
(6) Mikosch, J.; Trippel, S.; Eichhorn, C.; Otto, R.; Lourderaj, U.; Zhang, J. X.; Hase, W. L.; Weidemüller, M.; Wester, R. Imaging Nucleophilic Substitution Dynamics. *Science* **2008**, *319*, 183−186.
(7) Szabó, I.; Czakó, G. Revealing a Double-Inversion Mechanism for the F^- + CH_3Cl S_N2 Reaction. *Nat. Commun.* **2015**, *6*, 5972.
(8) Angel, L. A.; Ervin, K. M. Gas-Phase S_N2 and Bromine Abstraction Reactions of Chloride Ion with Bromomethane: Reaction Cross Sections and Energy Disposal into Products. *J. Am. Chem. Soc.* **2003**, *125*, 1014−1027.
(9) Wang, Y.; Song, H. W.; Szabó, I.; Czakó, G.; Guo, H.; Yang, M. H. Mode-Specific S_N2 Reaction Dynamics. *J. Phys. Chem. Lett.* **2016**, *7*, 3322−3327.
(10) van Bochove, M. A.; Swart, M.; Bickelhaupt, F. M. Nucleophilic Substitution at Phosphorus (S_N2@P): Disappearance and Reappearance of Reaction Barriers. *J. Am. Chem. Soc.* **2006**, *128*, 10738−10744.
(11) Manikandan, P.; Zhang, J. X.; Hase, W. L. Chemical Dynamics Simulations of X^- + CH_3Y → XCH_3 + Y^- Gas-Phase S_N2 Nucleophilic Substitution Reactions. Nonstatistical Dynamics and Nontraditional Reaction Mechanisms. *J. Phys. Chem. A* **2012**, *116*, 3061−3080.
(12) Bohme, D. K.; Mackay, G. I. Bridging the Gap Between the Gas-Phase and Solution: Transition in the Kinetics of Nucleophilic Displacement Reactions. *J. Am. Chem. Soc.* **1981**, *103*, 978−979.
(13) Vöhringer-Martinez, E.; Hansmann, B.; Hernandez, H.; Francisco, J. S.; Troe, J.; Abel, B. Water Catalysis of a Radical-Molecule Gas-Phase Reaction. *Science* **2007**, *315*, 497−501.
(14) Gertner, B. J.; Wilson, K. R.; Hynes, J. T. Nonequilibrium Solvation Effects on Reaction-Rates for Model S_N2 Reactions in Water. *J. Chem. Phys.* **1989**, *90*, 3537−3558.
(15) Tucker, S. C.; Truhlar, D. G. Effect of Nonequilibrium Solvation on Chemical Reaction Rates. Variational Transition-State-Theory

DOI: 10.1021/acs.jpclett.7b00577
J. Phys. Chem. Lett. 2017, 8, 1885−1892

Studies of the Microsolvated Reaction $Cl^-(H_2O)_n$ + CH_3Cl. *J. Am. Chem. Soc.* **1990**, *112*, 3347−3361.
(16) Laerdahl, J. K.; Uggerud, E. Gas Phase Nucleophilic Substitution. *Int. J. Mass Spectrom.* **2002**, *214*, 277−314.
(17) Tachikawa, H. Direct ab initio Molecular Dynamics Study on a Microsolvated S_N2 Reaction of $OH^-(H_2O)$ with CH_3Cl. *J. Chem. Phys.* **2006**, *125*, 133119.
(18) Regan, C. K.; Craig, S. L.; Brauman, J. I. Steric Effects and Solvent Effects in Ionic Reactions. *Science* **2002**, *295*, 2245−2247.
(19) Doi, K.; Togano, E.; Xantheas, S. S.; Nakanishi, R.; Nagata, T.; Ebata, T.; Inokuchi, Y. Microhydration Effects on the Intermediates of the S_N2 Reaction of Iodide Anion with Methyl Iodide. *Angew. Chem., Int. Ed.* **2013**, *52*, 4380−4383.
(20) Thomsen, D. L.; Reece, J. N.; Nichols, C. M.; Hammerum, S.; Bierbaum, V. M. Investigating the α-Effect in Gas-Phase S_N2 Reactions of Microsolvated Anions. *J. Am. Chem. Soc.* **2013**, *135*, 15508−15514.
(21) Hierl, P. M.; Ahrens, A. F.; Henchman, M.; Viggiano, A. A.; Paulson, J. F.; Clary, D. C. Nucleophilic Displacement as a Function of Hydration Number and Temperature: Rate Constants and Product Distributions for $OD^-(D_2O)_{0,1,2,3}$ + CH_3Cl at 200−500 K. *J. Am. Chem. Soc.* **1986**, *108*, 3142−3143.
(22) Otto, R.; Brox, J.; Trippel, S.; Stei, M.; Best, T.; Wester, R. Single Solvent Molecules can Affect the Dynamics of Substitution Reactions. *Nat. Chem.* **2012**, *4*, 534−538.
(23) Xie, J.; Otto, R.; Wester, R.; Hase, W. L. Chemical Dynamics Simulations of the Monohydrated $OH^-(H_2O)$ + CH_3I Reaction. Atomic-Level Mechanisms and Comparison with Experiment. *J. Chem. Phys.* **2015**, *142*, 244308.
(24) Fukui, K. The Path of Chemical Reactions - the IRC Approach. *Acc. Chem. Res.* **1981**, *14*, 363−368.
(25) Zhang, J. X.; Mikosch, J.; Trippel, S.; Otto, R.; Weidemüller, M.; Wester, R.; Hase, W. L. F^- + CH_3I → FCH_3 + I^- Reaction Dynamics. Nontraditional Atomistic Mechanisms and Formation of a Hydrogen-Bonded Complex. *J. Phys. Chem. Lett.* **2010**, *1*, 2747−2752.
(26) Mikosch, J.; Zhang, J. X.; Trippel, S.; Eichhorn, C.; Otto, R.; Sun, R.; de Jong, W. A.; Weidemüller, M.; Hase, W. L.; Wester, R. Indirect Dynamics in a Highly Exoergic Substitution Reaction. *J. Am. Chem. Soc.* **2013**, *135*, 4250−4259.
(27) Zhang, J. X.; Yang, L.; Xie, J.; Hase, W. L. Microsolvated $F^-(H_2O)$ + CH_3I S_N2 Reaction Dynamics. An Insight into the Suppressed Formation of Solvated Products. *J. Phys. Chem. Lett.* **2016**, *7*, 660−665.
(28) O'Hair, R. A. J.; Davico, G. E.; Hacaloglu, J.; Dang, T. T.; DePuy, C. H.; Bierbaum, V. M. Measurements of Solvent and Secondary Kinetic Isotope Effects for the Gas-Phase S_N2 Reactions of Fluoride with Methyl Halides. *J. Am. Chem. Soc.* **1994**, *116*, 3609−3610.
(29) Becke, A. D. Density-Functional Thermochemistry. III. The Role of Exact Exchange. *J. Chem. Phys.* **1993**, *98*, 5648−5652.
(30) The aug-cc-pVDZ basis set was used for the H, C, O, and F atoms. For iodine, the Wadt and Hay effective core potential (ECP) was used for the core electrons and an uncontracted 3s,3p basis set for the valence electrons. This iodine basis was augmented by a d-polarization function with a 0.262 exponent and s, p, and d diffuse functions with exponents of 0.034, 0.039, and 0.0873, respectively.[23,31,32] This basis is denoted as ECP/d in the text.
(31) Sun, R.; Davda, C. J.; Zhang, J. X.; Hase, W. L. Comparison of Direct Dynamics Simulations with Different Electronic Structure Methods. F^- + CH_3I with MP2 and DFT/B97−1. *Phys. Chem. Chem. Phys.* **2015**, *17*, 2589−2597.
(32) Xie, J.; Ma, X. Y.; Zhang, J. X.; Hierl, P. M.; Viggiano, A. A.; Hase, W. L. Effect of Microsolvation on the $OH^-(H_2O)_n$ + CH_3I Rate Constant. Comparison of Experiment and Calculations for $OH^-(H_2O)_2$ + CH_3I. *Int. J. Mass Spectrom.* **2016**, DOI: 10.1016/j.ijms.2016.10.017.
(33) Yang, L.; Liu, X.; Zhang, J. X.; Xie, J. Effect of Microsolvation on a S_N2 Reaction. Indirect Atomistic Dynamics and Weakened Suppression of Reactivity. *Phys. Chem. Chem. Phys.* **2017**, DOI: 10.1039/C7CP00294G.
(34) Xie, J.; Scott, M. J.; Hase, W. L.; Hierl, P. M.; Viggiano, A. A. Determination of the Temperature-Dependent $OH^-(H_2O)$ + CH_3I Rate Constant by Experiment and Simulation. *Z. Phys. Chem.* **2015**, *229*, 1747−1763.
(35) Zhang, J. X.; Yang, L.; Sheng, L. Electronic Structure Theory Study of the Microsolvated $F^-(H_2O)$ + CH_3I S_N2 Reaction. *J. Phys. Chem. A* **2016**, *120*, 3613−3622.
(36) Hiraoka, K.; Mizuse, S.; Yamabe, S. Solvation of Halide Ions with Water and Acetonitrile in the Gas Phase. *J. Phys. Chem.* **1988**, *92*, 3943−3952.
(37) Lemmon, E.; McLinden, M.; Friend, D.; Linstrom, P.; Mallard, W. *NIST Chemistry WebBook*; National Institute of Standards and Technology: Gaithersburg, MD. 2011.
(38) Ruscic, B. *Active Thermochemical Tables (ATcT)*. ATcT.anl.gov (2016).
(39) Pellerite, M. J.; Brauman, J. I. Intrinsic Barriers in Nucleophilic Displacements. *J. Am. Chem. Soc.* **1980**, *102*, 5993−5999.
(40) Hu, X.; Hase, W. L.; Pirraglia, T. Vectorization of the General Monte Carlo Classical Trajectory Program VENUS. *J. Comput. Chem.* **1991**, *12*, 1014−1024.
(41) Lourderaj, U.; Sun, R.; Kohale, S. C.; Barnes, G. L.; de Jong, W. A.; Windus, T. L.; Hase, W. L. The VENUS/NWChem Software Package. Tight Coupling between Chemical Dynamics Simulations and Electronic Structure Theory. *Comput. Phys. Commun.* **2014**, *185*, 1074−1080.
(42) Valiev, M.; Bylaska, E. J.; Govind, N.; Kowalski, K.; Straatsma, T. P.; van Dam, H. J. J.; Wang, D.; Nieplocha, J.; Apra, E.; Windus, T. L.; de Jong, W. A. NWChem: A Comprehensive and Scalable Open-Source Solution for Large Scale Molecular Simulations. *Comput. Phys. Commun.* **2010**, *181*, 1477−1489.
(43) Viggiano, A. A.; Arnold, S. T.; Morris, R. A.; Ahrens, A. F.; Hierl, P. M. Temperature Dependences of the Rate Constants and Branching Ratios for the Reactions of $OH^-(H_2O)_{0-4}$ + CH_3Br. *J. Phys. Chem.* **1996**, *100*, 14397−14402.
(44) Seeley, J. V.; Morris, R. A.; Viggiano, A. A. Temperature Dependences of the Rate Constants and Branching Ratios for the Reactions of $F^-(H_2O)_{0-5}$ with CH_3Br. *J. Phys. Chem. A* **1997**, *101*, 4598−4601.
(45) Su, T.; Morris, R. A.; Viggiano, A. A.; Paulson, J. F. Kinetic Energy and Temperature Dependences for the Reactions of Fluoride with Halogenated Methanes: Experiment and Theory. *J. Phys. Chem.* **1990**, *94*, 8426−8430.
(46) Jeffrey, G. A. *An Introduction to Hydrogen Bonding*; Oxford University Press: Oxford, U.K., 1977.
(47) Seeley, J. V.; Morris, R. A.; Viggiano, A. A.; Wang, H. B.; Hase, W. L. Temperature Dependence of the Rate Constants and Branching Ratios for the Reactions of $Cl(D_2O)_{1-3}$ with CH_3Br and Thermal Dissociation Rates for $Cl(CH_3Br)$. *J. Am. Chem. Soc.* **1997**, *119*, 577−584.

DOI: 10.1021/acs.jpclett.7b00577
J. Phys. Chem. Lett. 2017, 8, 1885−1892